Optik - International Journal for Light and Electron Optics 295 (2023) 171389

Contents lists available at ScienceDirect

Optik

journal homepage: www.elsevier.com/locate/ijleo

Original research article

Low-loss and high-sensitivity surface plasmon resonance sensor composed of microstructured optical fibers for wide visible-to-infrared and refractive index ranges

Xingdi Luo [a], Wei Liu [a], Jingwei Lv [a], Lin Yang [a], Qiang Liu [a], Jie He [a], Meiqi Liu [a], Paul K. Chu [b], Chao Liu [a,*]

[a] School of Physics and Electronic Engineering, Northeast Petroleum University, Daqing 163318, PR China
[b] Department of Physics, Department of Materials Science and Engineering, and Department of Biomedical Engineering, City University of Hong Kong, Tat Chee Avenue, Kowloon, Hong Kong Special Administrative Region

ARTICLE INFO

Keywords:
Microstructured fiber (MOF)
Surface plasmon resonance (SPR) sensor
Indium tin oxide (ITO) nanowires
Wide detection range
Low-loss transmission

ABSTRACT

Objective: Optical fiber sensing technology develops rapidly and is widely used. In order to design a SPR sensor with better performance and easy production, a new type D-MOF sensor with low loss, high sensitivity and simple structure is proposed.
Methods: The full vector finite element method (FEM) was used to optimize the structure parameters by using the multi-physics analysis software COMSOL, and the performance of the structure was systematically analyzed.
Results: The sensor operational wavelength spans the visible and infrared range (430 nm to 7200 nm). The refractive index detection range of 1.00–1.42, the maximum wavelength sensitivity and the optimal resolution are 60,000 nm/RIU and 1.67 × 10^{-6} RIU^{-1}, respectively, and the maximum limiting loss peak is 64.99 dB/cm. In addition, MOF-SPR sensors have large tolerance and low sensitivity of structural parameters in actual manufacturing. It has great application potential in biosensing and other fields.

1. Introduction

Surface plasmon resonance (SPR) is prevalent in many devices including absorbers, polarizers, and sensors in biomedicine, environmental monitoring, and chemical analysis [1–8] because of the rapid response, non-destructiveness, non-invasiveness, and high sensitivity to changes of analyte refractive indexes (RIs) [9–11]. The conventional prismatic SPR sensor relies on the total internal reflection (TIR) prism in the Kretschmann [12] and Otto [13] configurations as the optical couple. However, it has drawbacks such as complex apparatus, large volume, and susceptibility to mechanical influence [14,15]. Hence, smaller sensors with remote sensing capabilities are desirable. SPR sensors composed of ordinary optical fibers have been proposed [16] but it is challenging to control the coupling between the surface plasmon polaron (SPP) mode and core-guided mode and coupling losses and potential cross-sensitivity problems are prevalent. In comparison, the microstructured optical fiber (MOF) offers the flexibility to adjust the refractive indexes of the fiber core and cladding to more easily attain the phase matching conditions between the core-guided mode and surface plasmon mode. In addition, MOF-SPR sensors have other advantages such as single mode without cutoff, wide bandwidth, and high coupling

* Corresponding author.
E-mail address: msm-liu@126.com (C. Liu).

https://doi.org/10.1016/j.ijleo.2023.171389
Received 8 June 2023; Received in revised form 19 August 2023; Accepted 11 September 2023
Available online 14 September 2023

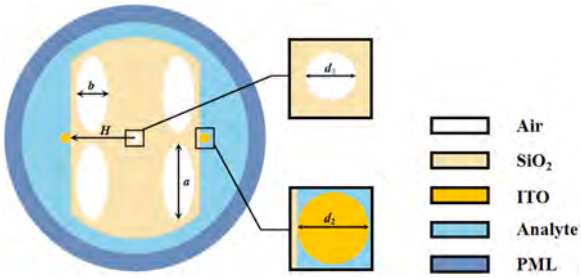

Fig. 1. Cross-section of the MOF-SPR sensor.

efficiency [17] and excitation of SPR can be achieved by selectively coating the MOF with a metal film or embedding metal nanowires [18]. However, the former process is relatively complex, and ensuring the uniformity of the metal coating can be challenging. On the other hand, metal nanowires fabricated on the outer surface of the fiber are more controllable in terms of dimensions and uniformity is usually not a concern, rendering them more viable in practice [19].

In order to improve the performance of the sensor, the choice of plasma material is very important. At present, silver, copper, and gold are selected as plasma materials to excite SPR in a large number of literatures. Silver has higher resonance peak, but its high oxidizing hindered its wide application in water environment. Copper faces the same problem. In addition, gold is not as conductive as silver and is expensive [16]. With the emergence of new plasma materials, indium tin oxide (ITO) has entered people's vision, and it has the advantages of oxidation resistance, low material cost, photoelectric characteristics controllable, and low loss in the infrared range, which greatly overcomes the shortcomings of traditional metal materials [20]. Therefore, ITO is selected as the plasma material in this paper.

The air holes of PCF are usually several microns in diameter, and the deposition of metal layers on their inner and outer surfaces requires high precision and complex processes [21]. Compared with metal thin films, nano-scale metal nanowires are small in size, which can limit their electrons and generate quantum effects, so they have strong absorption capacity for visible and near-infrared light [22]. Moreover, the nanowires structure simplifies the fabrication process [23]. Over the past few decades, the role of nanowires in sensing enhancement has been explored and further advances in technology have been made to make sensing structures simpler and more reliable [24,25].

In recent years, a variety of PCF-SPR sensors with nanowire structures have been proposed and numerically analyzed by the finite element method. In 2018, Liu et al. proposed a SPR probe based on photonic crystal fiber with gold nanowires as the plasmonic material. The maximum spectral sensitivity and confinement loss of the probe are 6000 nm/RIU and 120 dB/cm, respectively, and the detective RI range is between 1.27 and 1.36 [26]. In 2020, Tong et al. designed a biosensor based on SPR technology using silver nanowires as the sensing medium. Its maximum spectral sensitivity of 16000 nm/RIU, RI detection range of 1.32–1.38 and confinement loss peak of 350 dB/cm can be achieved [27]. In 2021, Kadhim et al. described a quasi-D-shape optical fiber sensor embedded with Au nanowires with a wavelength sensitivity of 14500 nm/RIU, RI detection range of 1.33–1.41, and confinement loss peak of 283.86 dB/cm [28]. However, these MOF sensors tend to show significant confinement losses consequently limiting their suitability in long-distance transmission. Additionally, their sensitivity is not high enough and the detectable RI range is rather narrow. To overcome these limitations and broaden the application scope, it is essential to develop MOF-SPR sensors with low confinement loss, high sensitivity, and a wider RI range.

Herein, an SPR-RI sensor based on MOF comprising external ITO nanowires is designed and analyzed by the full-vector finite element method (FEM). The sensor has fewer air holes in the cladding to simplify the manufacturing complexity and reduce the production cost. The external nanowires are positioned on both sides of the fiber to address the issue of coating inhomogeneity. The results reveal that the sensor has a maximum confinement loss of 64.99 dB/cm, average wavelength sensitivity (WS) of 15,571.23 nm/RIU, wide analyte refractive index (RI) detection range of 1.00–1.42, and maximum WS of up to 60,000 nm/RIU. The structure has excellent stability and can be operated in a wide wavelength range spanning 430 nm to 7200 nm. Owing to its simple structure, flexible design, convenient fabrication, and diverse functionalities, the sensor has significant practical potential. Our results demonstrate a notable breakthrough and innovation pertaining to the design and functionality of SPR sensors.

2. Design and theory of the MOF-SPR RI sensor

Surface plasmon resonance (SPR) is an optical phenomenon that occurs at the interface between the metal and medium [29]. When total internal reflection of incident light occurs at the interface with different refractive indexes, the evanescent wave is generated to produce coherent free electron oscillation on the metal surface and surface plasmon polaron (SPP) [30]. When the angle of the incident light is appropriate or the wavelength reaches a certain value, the incident light resonates with the plasmons on the metal surface, and a part of the energy of the incident light is transferred to the surface plasmons to propagate along the interface to form the surface plasma wave (SPW), resulting in a reduction of the energy of the reflected light [31] which can be observed from the transmission spectrum. When the refractive index of the medium on the metal surface changes, the resonant wavelength changes thus enabling the detection of small changes in the refractive indexes. To sum up, the MOF-SPR sensor makes use of a combination of micro-optical fiber technology, surface plasmon technology, and nanomaterials [32].

The cross-section of the MOF-SPR RI sensor is depicted in Fig. 1. The analyte solution is placed on the outer surface of the optical fiber cladding for the detection of RIs [19]. The cross-sectional structure is arranged in a square lattice, and the diameter of the cladding is 32 μm. There is a central air hole and four elliptical air holes in the cladding. The small air hole in the center of the fiber is mainly used to reduce the effective refractive index of the base film for better phase matching, whereas the four elliptical air holes provide better light confinement. The diameter of the central small air hole is $d_1 = 1.6$ μm, the major axis of the elliptical air hole is $a = 12$ μm, and the minor axis is $b = 4$ μm. Both sides of the fiber are polished to form two planes with a distance of $H = 10.5$ μm from the middle of the polished surface to the center of the fiber. In order to stimulate surface plasmon resonance, an indium tin oxide nanowire is placed at the middle point of the polished surface. The diameter of the indium tin oxide nanowire is $d_2 = 1.6$ μm, and it is tangent to the middle point of the polished surface. The sensor is made of silica, and the combination of silica and indium tin oxide improves the sensing properties of the MOF-SPR sensor. The sensor is designed with a perfect matching layer (PML) and the refractive index of PML is the same as that of silica. The refractive index of silica is calculated by Eq. (1) [33]:

$$n(\lambda) = \sqrt{1 + \frac{A_1\lambda^2}{\lambda^2 - B_1} + \frac{A_2\lambda^2}{\lambda^2 - B_2} + \frac{A_3\lambda^2}{\lambda^2 - B_3}}, \tag{1}$$

where $A_1 = 0.696166300$, $A_2 = 0.407942600$, $A_3 = 0.897479400$, $B_1 = 4.67914826 \times 10^{-3}$ μm^2, $B_2 = 1.35120631 \times 10^{-2}$ μm^2, and $B_3 = 97.9340025$ μm^2 and λ is the wavelength of the incident light in vacuum. The wavelength dependence of the dielectric constant of the ITO films is calculated according to the Drude model [20] by Eq. (2):

$$\varepsilon_m(\lambda) = \varepsilon_\infty - \frac{\lambda^2\lambda_c}{\lambda_p^2(\lambda_c + i\lambda)}, \tag{2}$$

where $\lambda_p = 5.6497 \times 10^{-7}$ m and $\lambda_c = 11.21076 \times 10^{-6}$ m are the plasma wavelength of ITO and collision wavelength of ITO, respectively, $\varepsilon_\infty = 3.80$ is the dielectric constant of the infinite value of ITO frequency, and λ is the working wavelength in μm.

The confinement loss with a unit of dB/cm is an important property of the sensor and calculated [34] by Eq. (3):

$$\alpha_{loss} = 8.686 \times \frac{2\pi}{\lambda} \mathrm{Im}(n_{eff}) \times 10^4, \tag{3}$$

where λ is the wavelength in μm, $\mathrm{Im}(n_{eff})$ is the imaginary part of the effective refractive index of the fundamental mode, and α_{loss} is the confinement loss value. The wavelength sensitivity is calculated by the wavelength inquiry method and amplitude inquiry method. The wavelength sensitivity with a unit of nm/RIU [35] is calculated by Eq. (4):

$$S_\lambda(\lambda) = \frac{\Delta\lambda_{peak}}{\Delta n_a}, \tag{4}$$

where $\Delta\lambda_{peak}$ is peak wavelength shift, Δn_a is the variation of the refractive index (RI). The amplitude sensitivity is calculated by Eq. (5) [36]:

$$S_A(RIU^{-1}) = -\frac{1}{\alpha(\lambda, n_a)} \frac{\partial\alpha(\lambda, n_a)}{\partial n_a}, \tag{5}$$

where $\alpha(\lambda, n_a)$ is the confinement loss of the analyte RI and $\partial\alpha(\lambda, n_a)$ is the difference of the confinement loss of two adjacent RI of two analytes.

The figure of merit (FOM) is another important parameter of the SPR fiber optic sensor to gauge the overall performance. The FOM is calculated by Eq. (6) [37]:

$$FOM = \frac{S_n}{FWHM}, \tag{6}$$

where S_n is the wavelength sensitivity and FWHM is the full-width at half-maximum that represents the band length corresponding to half the height of the formant [38]. The resolution is another important parameter that is determined by Eq. (7) [39,40]:

$$R(RIU) = \Delta n_a \times \Delta\lambda_{min} / \Delta\lambda_{peak}, \tag{7}$$

where $\Delta\lambda_{peak}$ refers to the peak wavelength displacement, Δn_a is the variation of analyte RI, and $\Delta\lambda_{min}$ is the spectrometer resolution which is generally set at 0.1 nm.

The finite element method is adopted to analyze the structure based on the COMSOL multi-physics software. The simulated region is a free triangular mesh and to improve the accuracy, a hypothetical perfect matching layer (PML) is introduced to the edge of the analyte to absorb the scattered energy [41].

3. Mode selection and optimal structural parameters

In sensing, the optical fiber usually has two modes: X mode and Y mode. The X mode is further divided into the X odd mode and X even mode, and the Y mode is into the Y odd mode and Y even mode [42]. Fig. 2(a), (b), (c), (d), and (e) display the electric field distributions of the odd mode of X, even mode of X, odd mode of Y, even mode of Y, and SPP mode, respectively.

Fig. 2(f) and (g) are the electric field diagrams under the mode coupling of single D-type and double D-type sensors, respectively. Fig. 2(f) shows the fiber sensing structure with unilateral polishing (single D-type). The electric field diagram reflects that in the single D sensing structure, the energy in the fiber core is transferred to only one side of the nanowire. Compared with the single D-type sensor structure, the energy in the fiber core is transferred to the nanowires on both sides of the structure at the same time, which greatly improves the coupling efficiency between fundamental mode and plasmonic mode, further stimulates the SPR better, and improves the output characteristics of the sensor.

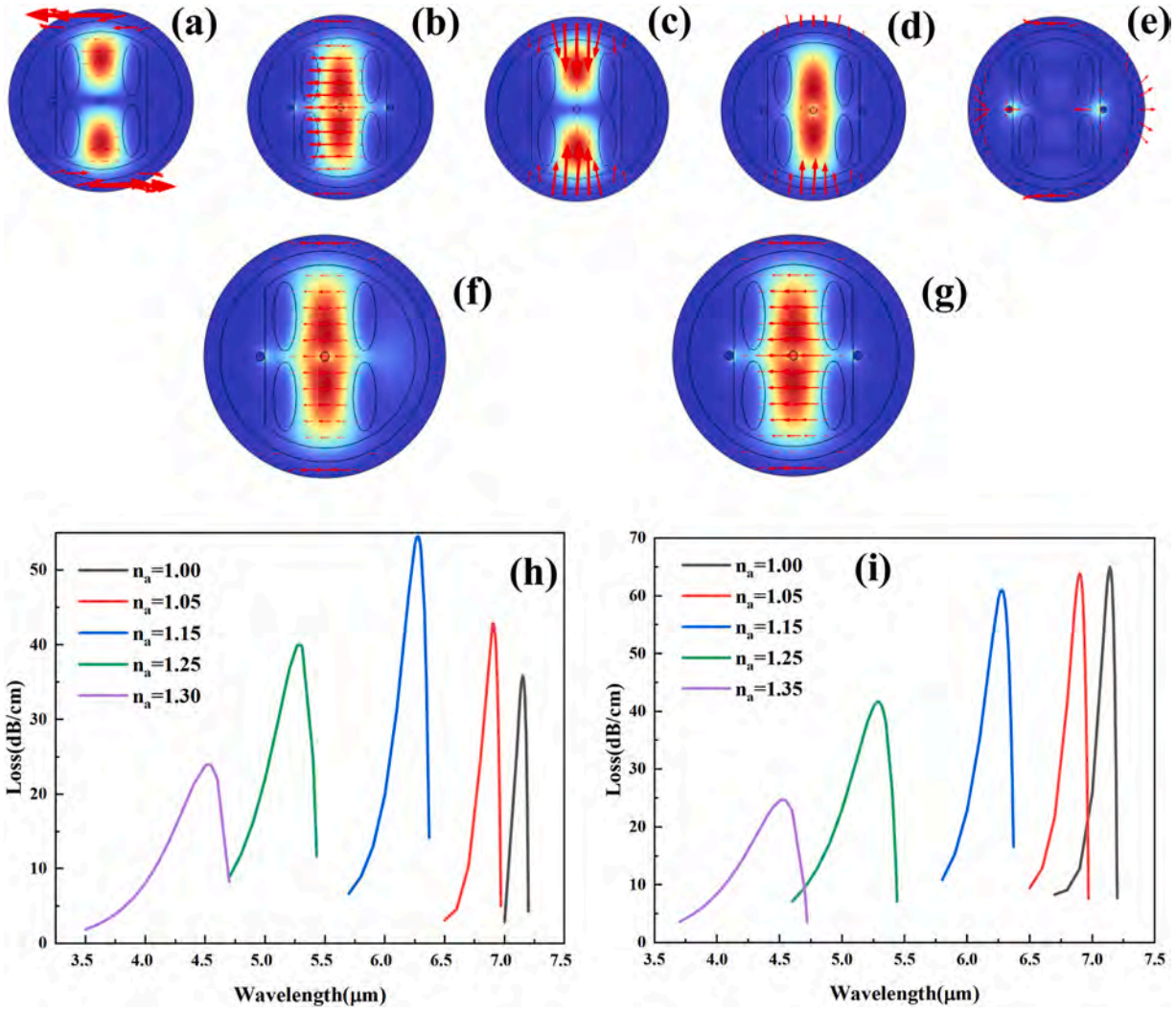

Fig. 2. (a-d) Electric field distributions of the base films in different modes and (e) Electric field distributions of the SPP mode corresponding to the X even mode, (f) and (g) are the electric field diagrams under the mode coupling of single D type and double D type sensors respectively, (h) and (i) are the loss plots of the single D and double D types, respectively.

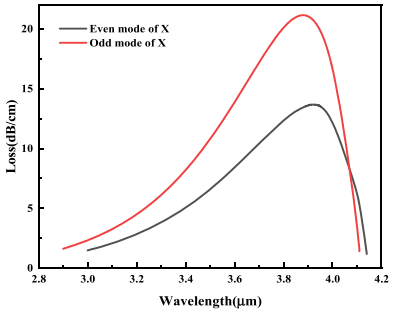

(A)

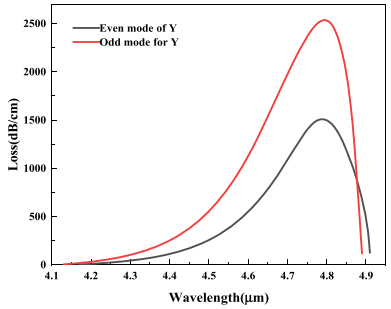

(B)

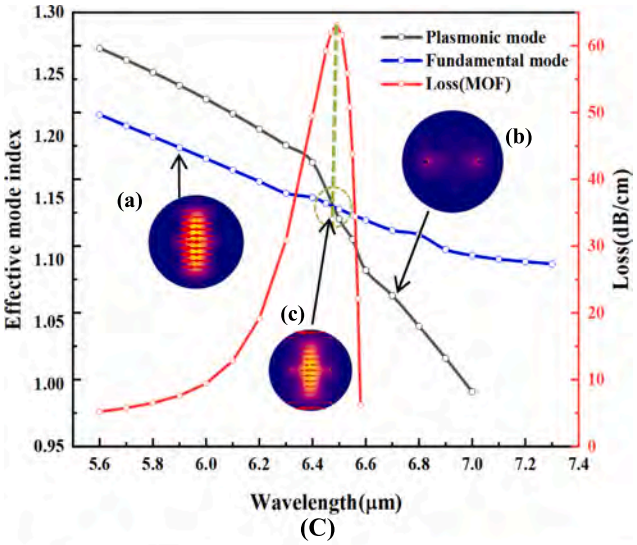

(C)

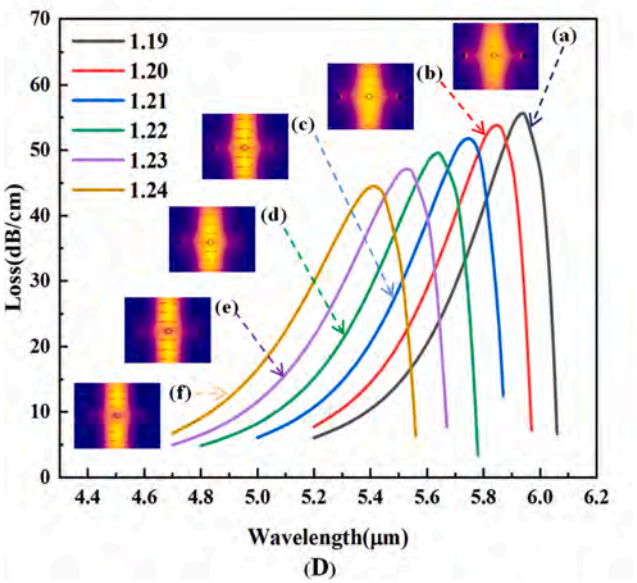

(D)

(caption on next page)

Fig. 3(. A) and (B) show the confinement loss curves of the X even and X odd modes as well as the Y even and Y odd modes as a function of the wavelength for a refractive index of $n_a = 1.33$, respectively. The X even mode and X odd mode show the confinement loss peaks at 3.92 μm and 3.90 μm, respectively, and the Y-even mode and Y-odd mode at of 4.8 μm. The resonant wavelength of the Y mode is obviously longer thereby requiring a stronger light source. In addition, the confinement loss peak of the X mode is smaller than that of the Y mode, and the detection distance of the X mode is longer. The advantages of the X mode are obvious and the X mode is thus chosen in our investigation. Compared to the confinement loss peaks of the X-odd mode and X even mode, that of the X odd mode is slightly smaller, but the wavelength sensitivity of the X-even mode is higher resulting in better sensing performance. Therefore, the X-even mode is selected to analyze the characteristics of the sensor.

Fig. 2(h) and (i) show the loss curves of the single D-type sensing structure and the double D-type sensing structure under the same condition at different refractive indices, respectively. Through the comparison, it can be seen that the loss peak of the resonance coupling curve for the single D-type sensing structure rises first and then decreases with the analytes RIs increasing, and the overall does not have monotonicity. In the double D-type sensing structure, the loss peak of the resonance coupling curve increases with the increase of refractive indices, which has strict monotonicity. It has important guiding value for the sensor to present outstanding optical performance [16].

To sum up, the double D-type sensing structure is finally selected for research and analysis.

Fig. 3. (A) CL spectra of the X even mode and X odd mode; (B) CL spectra of the Y even mode and Y odd mode; (C) Dispersion relations of the fundamental core mode, SPP mode, and confinement loss spectra for $n_a = 1.10$; (D) Loss curve with RIs in the range of 1.19–1.24, and the electric field diagrams corresponding to the resonance loss peaks.

As shown in Fig. 3 (C), the coupling mechanism between the fundamental mode and the plasmonic mode is described, including curves and electric field distributions, which are the basis for subsequent analysis of sensor performance and applications. In general, the physical parameters of dispersion and confinement loss are related to the real and imaginary parts of the effective refractive index, respectively. The black and blue dashed lines represent the $Re(n_{eff})$ of the plasmonic mode and the fundamental mode, and the red dashed lines represent the fundamental mode CL associated with $Im(n_{eff})$. As the wavelength gradually increases, the $Re(n_{eff})$ of the two modes decreases at different rates, having the same $Re(n_{eff})$ at 6490 nm, and at the same time, the maximum loss peak appears at the intersection of the two curves, which meet the phase matching conditions [17]. Inset (a), (b) and (c) show the electric field distribution for the different cases. Before coupling occurs, the energy is present only at the core (inset (a)) and the ITO nanowire (inset (b)). After coupling, a part of the energy is transferred from inside the core (inset (a)) to the nanowires (inset (b)) to further achieve resonance (inset (c)). Therefore, the combination of relation curve and electric field distribution illustrates the basic principle and significance of SPR.

The loss curves and the electric field distributions with the analyte RIs in the range of 1.19–1.24 are shown in Fig. 3 (D). Inset (a)-(f) stand for the electric field diagrams at the resonance loss peaks of detective RIs region between 1.19 and 1.24. This figure is indicated the weakening of the coupling effect between modes as the analyte RIs gradually increases.

The influence of different structural parameters on the sensing properties is analyzed for an analyte RI of 1.33. Fig. 4(a) shows the confinement loss spectra for different diameters of the central air hole d_1. When d_1 is 1.6 μm, the confinement loss peak is the highest. When the limiting loss peak is in a lower range, structural parameters with higher confinement loss peaks are obtained to better excite surface plasmon resonance (SPR). Therefore, $d_1 = 1.6$ μm is selected. As shown in Fig. 4(b) and (c), when the long axis a and short axis b of the elliptical air hole are changed from 9 to 13 μm and 1–5 μm, respectively, the resonance wavelength blue-shifts and the confinement loss peaks change. The change of the major axis has a small effect on the confinement loss peak, but the change in the minor axis b has a relatively large influence on the confinement loss peak. When a is 12 μm, the confinement loss peak is the largest so that SPR can be excited more effectively. Hence, 12 μm is selected as the optimal value of the long axis of the elliptical air hole. Although the confinement loss peak of the minor axis b of 4 μm is not as large as that of the minor axis b of 5 μm, the wavelength sensitivity of the minor axis b of 4 μm is high. After consideration, b of 4 μm is selected as the optimal value of the minor axis of the elliptical air hole. Fig. 4(d) presents the influence of different diameters of the indium tin oxide nanowires on the constrained loss spectra. When the nanowire diameter d_2 is varied from 0.8 μm to 1.6 μm, the change in the nanowire diameter has little effect on the confinement loss peaks. When d_2 is 1.6 μm, the confinement loss is relatively large and the wavelength sensitivity is high. Hence, 1.6 μm is selected as the optimal value for the nanowire diameter. Fig. 4(e) shows the influence of different polishing degrees on the confinement loss spectra. When the distance H from the middle of the polished surface to the center of the fiber is varied from 10.5 μm to 14.5 μm, the change in H has little influence on the confinement loss peaks. When H is 10.5 μm, the sensor has the maximum confinement loss peak and highest wavelength sensitivity. By considering the manufacturing difficulty, 10.5 μm is chosen as the optimal value of H. All in all, the structural sensitivity is small consequently giving rise to large tolerance or margin of error in manufacturing which can be made simpler and more cost-effective [43]. In summary, the optimal structural values of d_1, a, b, d_2, and H are 1.6 μm, 12 μm, 4 μm, 1.6 μm, and 10.5 μm, respectively.

The characteristics of the sensor are determined using a refractive index step size of 0.01 in the RI range of 1.00 RIU to 1.42 RIU. As the refractive index goes up, the resonance wavelength blue-shifts, and the peak of the confinement loss decreases gradually with

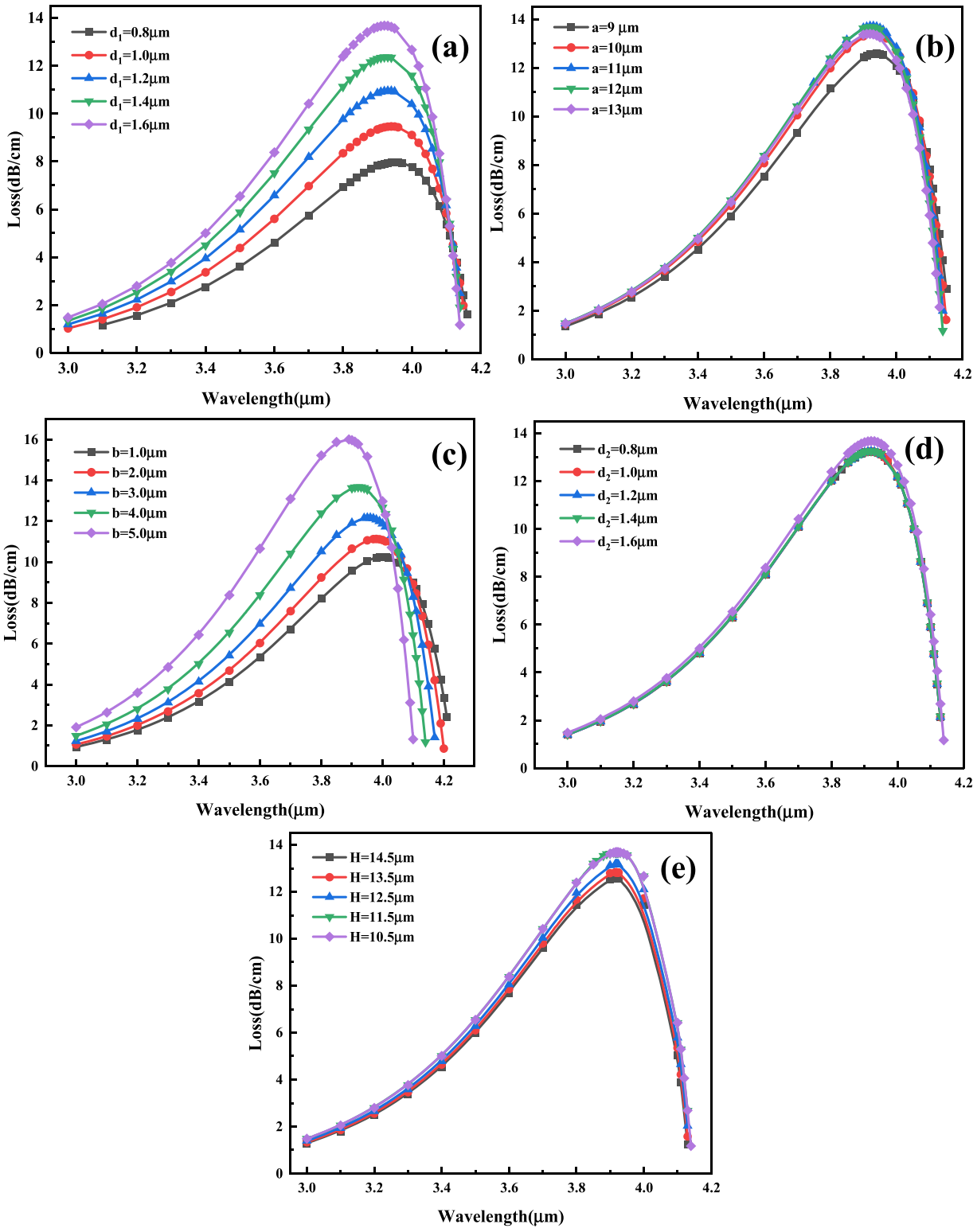

Fig. 4. Dependence of CL on wavelengths for different structural parameters.

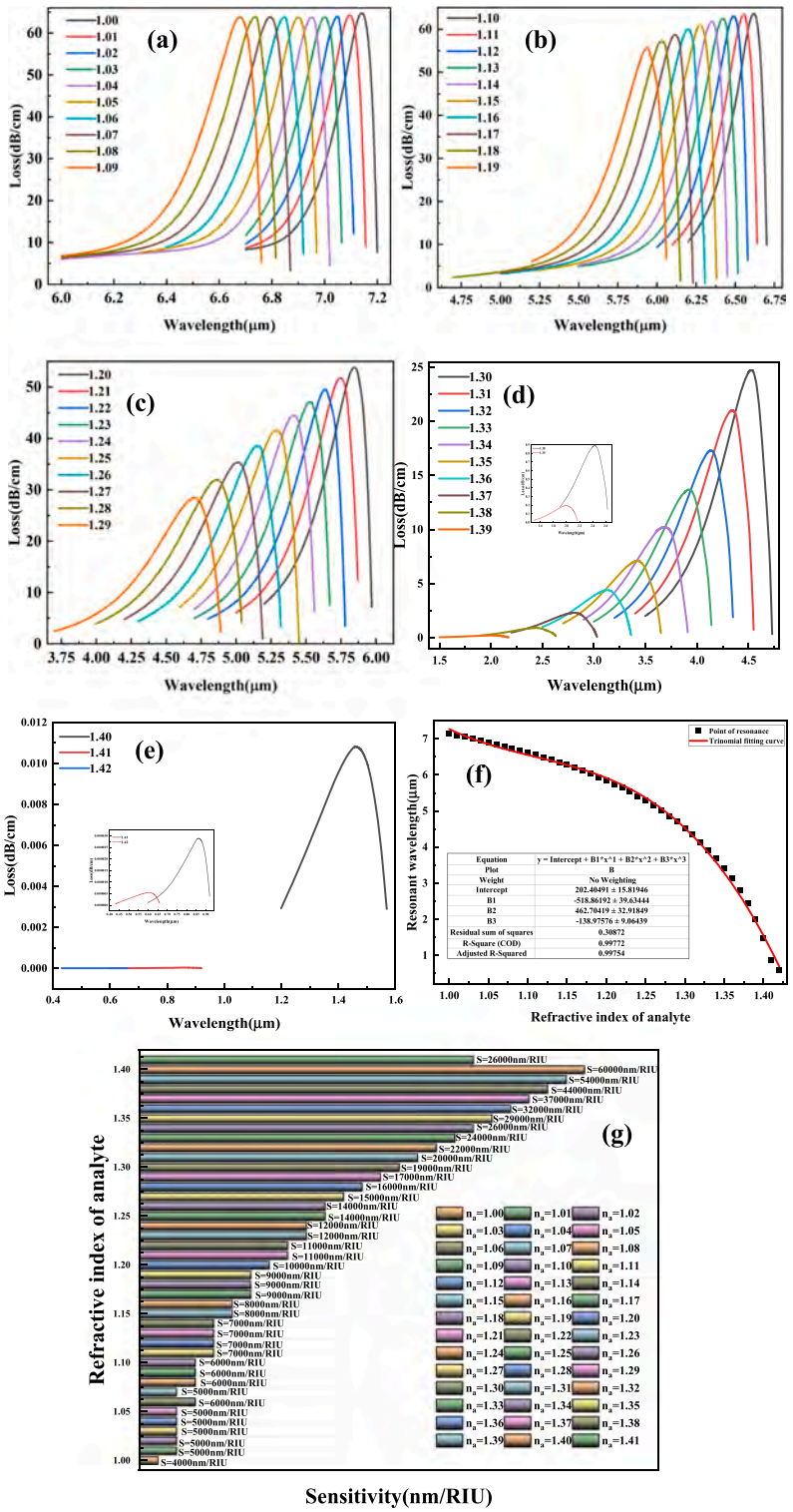

Fig. 5. CL spectra with changing wavelengths for different analyte RIs: (a) 1.00–1.09, (b) 1.10 – 1.19, (c) 1.20–1.29, (d) 1.30–1.39, and (e) 1.40–1.42; (f) Fitted linear relationship between the resonance wavelength and analyte refractive index; (g) Wavelength sensitivity of the formants for different analyte refractive indexes.

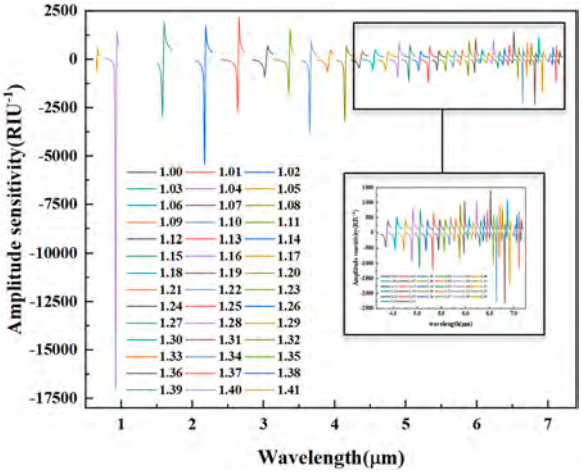

Fig. 6. Amplitude sensitivity of the resonant peaks.

increasing refractive indexes. When the refractive indexes are between 1.00 and 1.11, the peak confinement loss does not change significantly. However, when the refractive index is between 1.12 and 1.42, the confinement loss peak decreases gradually because SPR occurs when the core guide mode and SPP mode meet the phase-matching conditions. When the liquid analyte refractive index changes, the phase-matching conditions change as well resulting in a blue shift in the resonance wavelength. The confinement loss for refractive indexes between 1.00 and 1.42 are shown in Fig. 5(a), (b), (c), (d), and (e). The CL values are calculated by Eq. (3). The $n_a$confinement loss spectra increase initially and then decrease as the wavelength blue-shifts. The variation in the analyte refractive indexes with resonance wavelength and the nonlinear fitting in Fig. 4(f) reveal a good continuous response. The adjusted R of the fit is 0.99754 indicating the ability to accurately detect the analyte. The polynomial fit for the refractive index range from 1.00 to 1.42 is: $\lambda_R(nm) = 202404.91 - 518861.92n_a + 462704.19n_a^2 - 138975.76n_a^3$. For $1 \leq n_a \leq 1.42$, where λ_R represents the resonance wavelength and n_a is the refractive index of the solution being measured. The effective refractive index range is 1.00–1.42. When the refractive index is greater than 1.42, the CL is close to zero and the CL curves are irregular while the wavelength sensitivity diminishes greatly. The wavelength sensitivity is proportional to the refractive index in the range of 1.00–1.41. The wavelength sensitivity is calculated by Eq. (4). When the RI of the liquid changes from 1.40 to 1.41, the maximum wavelength sensitivity is 60,000 nm/RIU, and when the RI changes from 1.00 to 1.01, the minimum wavelength sensitivity is 4000 nm/RIU. The mean wavelength sensitivity in the refractive index range of 1.00–1.42 is 15,571.43 nm/RIU. Fig. 5(g) summarizes the wavelength sensitivities for different analytes refractive indexes shown in (a)-(e).

Although it is common to use the wavelength sensitivity to determine the sensing performance, processing of the CL spectra for different analytes is quite complicated. In fact, it can be accomplished by observing different analytes for a fixed wavelength change of the transmission light power. This simpler and less costly method is amplitude questioning. The amplitude sensitivity is calculated by Eq. (5) and the amplitude sensitivity is shown in Fig. 6. The amplitude sensitivity for most n_a increases first and then decreases. In addition, the wavelength blue-shifts with increasing RIs. The maximum amplitude sensitivity is observed for n_a of 1.40, indicating that the sensor is extremely sensitive to analytes with n_a of 1.40.

In practical applications, owing to inevitable variations in the actual operation, temperature, stress, and other external factors, the actual performance of the optical fiber may deviate from the theoretical predictions. In fact, small changes in the optical fibers may lead to significant changes in the sensing characteristics [43] and MOF-SPR sensors with large manufacturing tolerance or margin of error are more practical. Here, the structural parameter sensitivity is adopted to analyze the stability of the SPR sensor from the perspective of commercial production. The lower the structural sensitivity, the greater the tolerance, and the better the stability of the sensor. For n_a equal to 1.33, the structural sensitivity of the small central air hole diameter d_1, major axis a, minor axis b of the ellipse, outer indium tin oxide nanowires diameter d_2, and distance H from the midpoint of the polished surface to the center of the fiber is determined and discussed. As shown in Fig. 7(a) to (e), with respect to the resonant wavelength shown in the diagram, only tiny changes are observed for these parameters. For example, when d_2 changes from 0.8 μm to 1.4 μm, the resonance wavelength hardly changes, and when d_2 changes from 1.4 μm to 1.6 μm, the resonance wavelength only changes slightly. Therefore, the sensor sensitivity has large manufacturing tolerance and the stability is good.

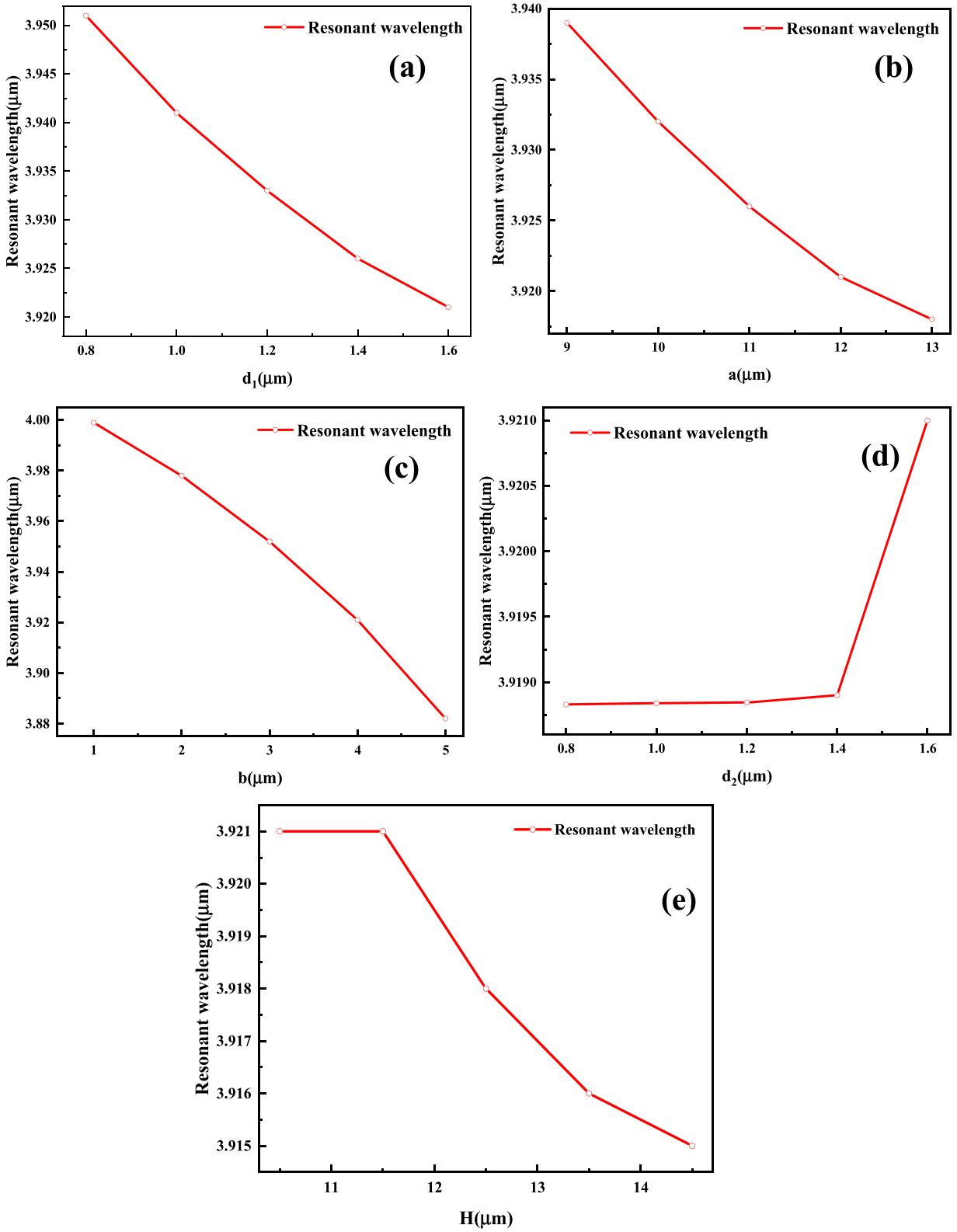

Fig. 7. Structural parameter sensitivity: (a) Diameter of the central air hole, (b) Major axis of the elliptical air hole, (c) Minor axis of the elliptical air hole, (d) Diameter of the ITO nanowires, and (e) Polishing depth H for an analyte refractive index of 1.33.

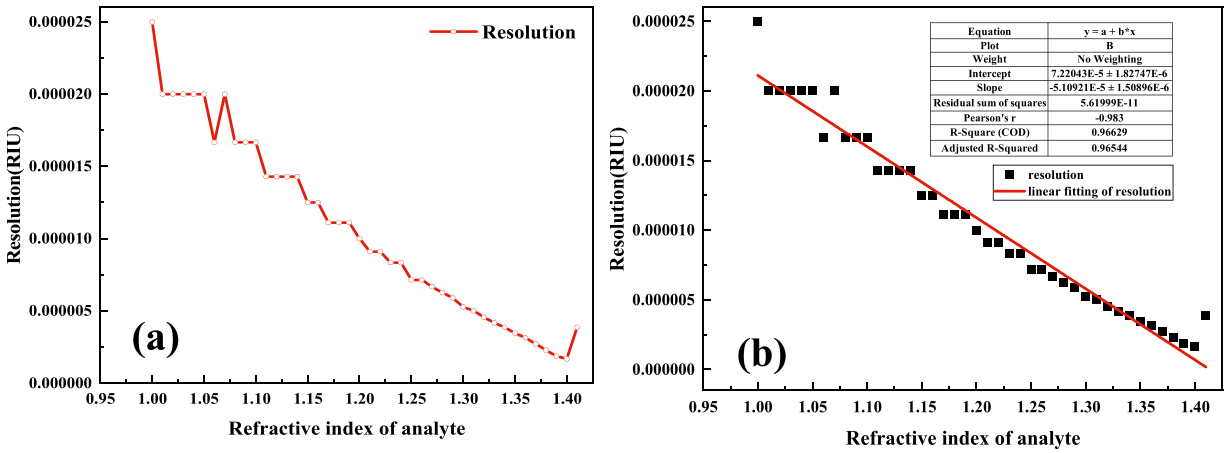

Fig. 8. Resolution of the MOF-SPR sensor and linear fitting.

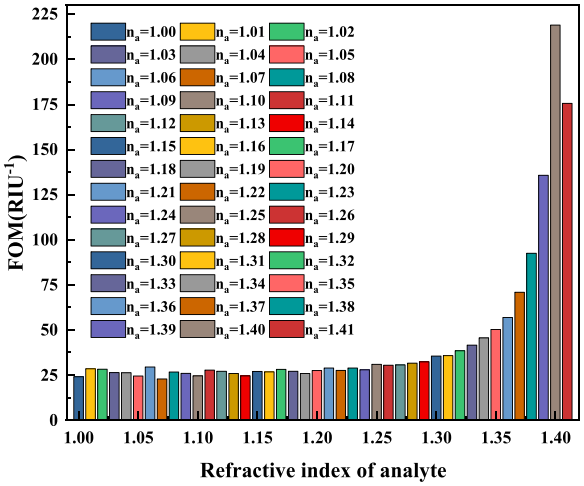

Fig. 9. Variations of FOM with analyte RI.

The resolution is another key entity dictating the ability to detect minimal changes [44]. According to Eq. (7), the resolution is inversely proportional to the wavelength sensitivity. Fig. 8(a) and (b) show the resolution and linear fit of the formants, respectively. When the analyte refractive indexes increase, the resolution of the formants decreases gradually and the ability to detect weak signal changes improves gradually. The optimal resolution is 1.67×10^{-6} RIU and the empirical equation is $R(RIU) = -5.11 \times 10^{-5} + 7.22 \times 10^{-5}\ n_a$ with R^2 of 96.63%.

The figure of merit (FOM) is often used to evaluate the overall performance of the sensor. The larger the FOM, the better the comprehensive performance of the MOF-SPR sensor [43]. The FOM can be calculated by Eq. (6) and Fig. 9 shows the FOM changes at the resonance peak. When n_a is less than or equal to 1.40, the FOM increases gradually with refractive indexes, but when n_a is greater than or equal to 1.40, FOM decreases. When n_a is 1.40, FOM is the largest indicating the best sensing performance here.

Table 1 compares the optical properties of MOF-SPR sensors recently investigated. The choice of plasmonic materials is very important to the sensor performance. The table lists a series of sensors with conventional gold, silver, as well as novel ITO nanowires as the sensing mediums. Compared with the previously proposed sensors, this sensor can detect large RI analytes in a wider visible-to-infrared wavelength region with higher sensitivity. Therefore, the recommended sensor delivers better output peculiarity performance in the field of biochemical sensing.

The analysis of manufacturing tolerance can well analyze the error caused by the manufacturing process difference to the structure, and can reflect the stability and feasibility of the device [45]. General manufacturing tolerances range from ± 2% to ± 10%. As shown

Table 1
Performance comparison with recently reported sensors.

Refs.	Fiber structure	Metal	RI range	Sensitivity (nm/RIU)	Resolution (RIU)	Str. diagram
[21]	Dual PCF	Au	1.13–1.35	17,500	5.71×10^{-6}	
[25]	Ex-core PCF	Au	1.33–1.40	14,200	7.04×10^{-6}	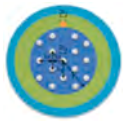
[26]	Single-core PCF	Au	1.27–1.36	6,000	1.67×10^{-5}	
[27]	Dual-core PCF	Ag	1.32–1.38	16000	6.25×10^{-6}	
[28]	D-shaped PCF	Au	1.33–1.41	14,500	6.90×10^{-6}	
Ours	Dual-core MOF	ITO	1.00–1.42	60,000	1.67×10^{-6}	

in Fig. 10, we analyze the manufacturing tolerance of ± 5% of the proposed sensor. Fig. 10(a) is the long axis analysis diagram of the elliptical air hole. When a changes at about 12 μm, the resonance wavelength does not change, and the resonance loss changes by 0.21 dB/cm; Fig. 10(b) shows the short-axis analysis diagram of the elliptical air hole. When b changes at about 4 μm, the resonance wavelength changes by 20 nm and the resonance loss changes by 0.73 dB/cm; Fig. 10(c) is the analysis diagram of the diameter of the central air hole. When d_1 changes at about 1.6 μm, the resonance wavelength does not changed, and the resonance loss changes by 1 dB/cm; Fig. 10(d) shows the nanowire diameter analysis diagram. When d_2 changes at about 1.6 μm, the resonance wavelength does not change, and the resonance loss changes by 0.42 dB /cm; Fig. 10(e) is the D-type polishing depth analysis diagram. When H changes at about 10.5 μm, the resonance wavelength does not changed, and the resonance loss changes by 0.44 dB /cm. These changes are essentially negligible compared to itself. In summary, the sensor can effectively reduce the appropriate interference due to the manufacturing process.

4. Conclusion

A surface plasmon resonance (SPR) microstructured fiber (MOF) sensor containing indium tin oxide (ITO) nanowires is designed and analyzed. The sensor has many distinct advantages such as low loss, high sensitivity, and wide RI detection range (430 nm to 7200 nm). The maximum wavelength sensitivity and resolution for $n_a = 1.40$ are 60,000 nm/RIU and 1.67×10^{-6} RIU^{-1}, respectively. The low confinement loss facilitates long-distance transmission and detection of a wide range of analyte RIs (1.00 – 1.42). More importantly, the simple design with high structural tolerance reduces the manufacturing complexity and cost. In the near-infrared regime, the penetration depth of the evanescent field is greater and the sensor has enormous potential in NIR bio-molecular and organic applications.

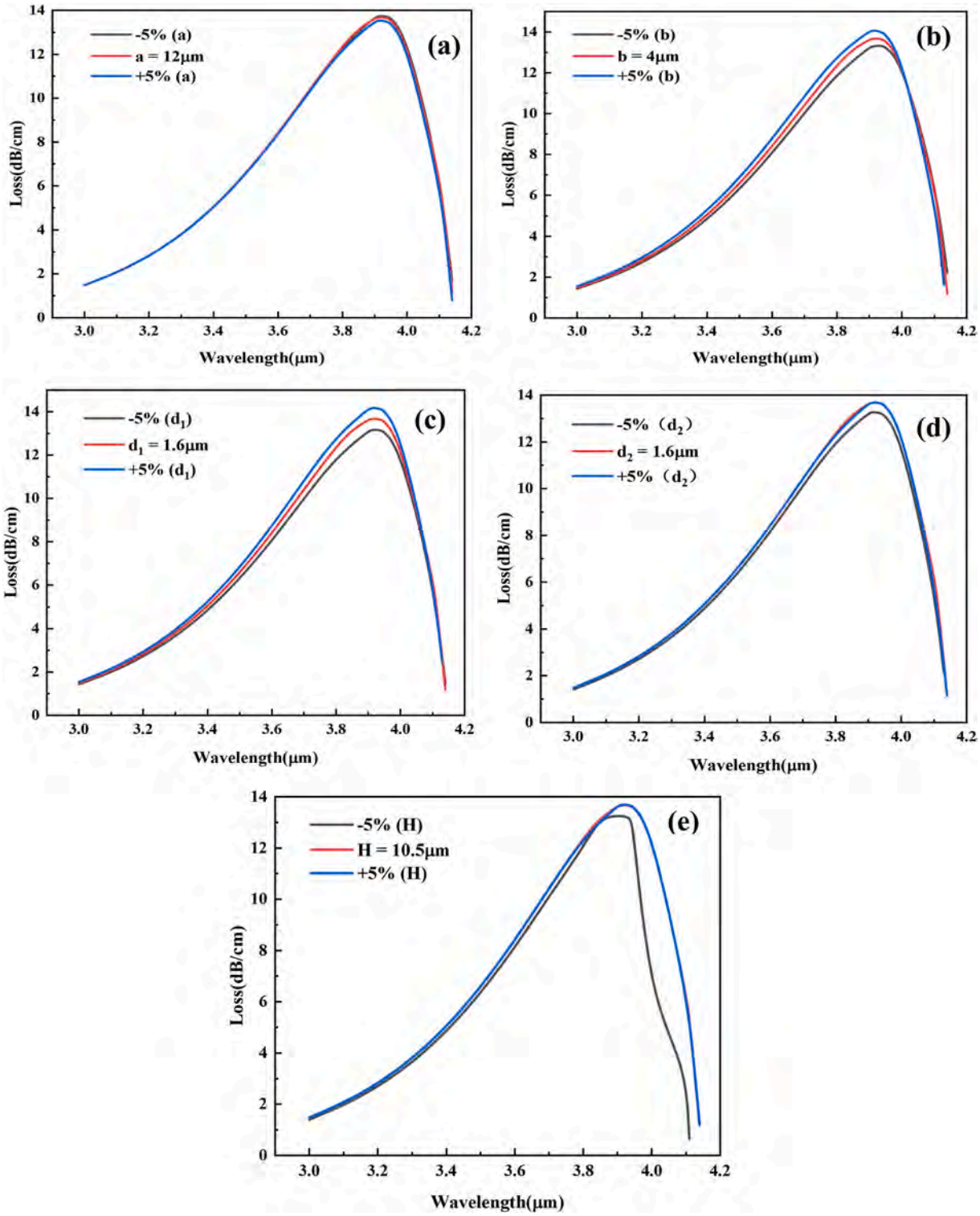

Fig. 10. Manufacturing tolerance analysis. (a) Major axis of the elliptical air hole, (b) Minor axis of the elliptical air hole, (c) Diameter of the central air hole, (d) Diameter of the ITO nanowires, and (e) D-type polishing depth H analysis.

Declaration of Competing Interest

The authors declare no conflicts of interest.

Data availability

The authors do not have permission to share data.

Acknowledgments

This work was jointly supported by Heilongjiang Provincial Natural Science Foundation of China [JQ2023F001], Outstanding young and middle-aged research and innovation team of Northeast Petroleum University [KYCXTD201801], Local Universities Reformation and Development Personnel Training Supporting Project from Central Authorities, Postdoctoral Scientific Research Development Fund of Heilongjiang Province (LBH-Q20081), City University of Hong Kong Donation Research Grant [DON-RMG No. 9229021], City University of Hong Kong Strategic Research Grant [SRG 7005505], and City University of Hong Kong Donation Grant [9220061].

References

[1] W. Liu, Y. Shi, Z. Yi, C. Liu, F.M. Wang, X.L. Li, J.W. Lv, L. Yang, P.K. Chu, Surface plasmon resonance chemical sensor composed of a microstructured optical fiber for the detection of an ultra-wide refractive index range and gas-liquid pollutants, Opt. Express 29 (25) (2021) 40734–40747.
[2] P. Yu, X. Chen, Z. Yi, Y. Tang, H. Yang, Z. Zhou, T. Duan, S. Cheng, J. Zhang, Y. Yi, A numerical research of wideband solar absorber based on refractory metal from visible to near infrared, Opt. Mater. 97 (2019), 109400.
[3] C. Liang, Y. Zhang, Z. Yi, X. Chen, Z. Zhou, H. Yang, Y. Yi, Y. Tang, W. Yao, Y. Yi, A broadband and polarization-independent metamaterial perfect absorber with monolayer Cr and Ti elliptical disks array, Results Phys. 15 (2019), 102635.
[4] F. Qin, Z. Chen, X. Chen, Z. Yi, W. Yao, T. Duan, P. Wu, H. Yang, G. Li, Y. Yi, A tunable triple-band near-infrared metamaterial absorber based on Au nanocuboids array, Nanomaterials 10 (2) (2020) 207.
[5] Z.P. Zheng, Y. Zheng, Y. Luo, Z. Yi, J.G. Zhang, Z.M. Liu, W.X. Yang, Y. Yu, X.W. Wu, P.H. Wu, A switchable terahertz device combining ultra-wideband absorption and ultra-wideband complete reflection, Phys. Chem. Chem. Phys. 24 (2022) 2527–2533.
[6] Z.P. Zheng, Y. Luo, H. Yang, Z. Yi, J.G. Zhang, Q.J. Song, W.X. Yang, C. Liu, X.W. Wu, P.H. Wu, Thermal tuning of terahertz metamaterial absorber properties based on VO2, Phys. Chem. Chem. Phys. 24 (2022) 8846–8853.
[7] F.Q. Zhou, F. Qin, Z. Yi, W.T. Yao, Z.M. Liu, X.W. Wu, P.H. Wu, Ultra-wideband and wide-angle perfect solar energy absorber based on Ti nanorings surface plasmon resonance, Phys. Chem. Chem. Phys. 213 (2021) 17041–17048.
[8] X. Yan, R. Fu, T.L. Cheng, S.G. Li, A highly sensitive refractive index sensor based on a V-Shaped photonic crystal fiber with a high refractive index range, Sensors 21 (2021) 3782.
[9] X.X. Wang, J.K. Zhu, H. Tong, X.D. Yang, X.X. Wu, Z.Y. Pang, H. Yang, Y.P. Qi, A theoretical study of a plasmonic sensor comprising a gold nano-disk array on gold film with an SiO_2 spacer, Chin. Phys. B 28 (4) (2019), 044201.
[10] T.S. Li, L.Q. Zhu, X.C. Yang, X.P. Lou, L.D. Yu, A refractive index sensor based on H-shaped photonic crystal fibers coated with Ag-graphene layers, Sensors 20 (3) (2020) 741.
[11] C. Liu, J.W. Wang, F.M. Wang, W.Q. Su, L. Yang, J.W. Lv, G.L. Fu, X.L. Li, Q. Liu, T. Sun, P.K. Chu, Surface plasmon resonance (SPR) infrared sensor based on D-shape photonic crystal fibers with ITO coatings, Opt. Commun. 464 (2020), 125496.
[12] E. Kretschmann, H. Raether, Radiative decay of non-radiative surface plasmons excited by light, Z. Naturforsch. A 23 (1968) 2135.
[13] A. Otto, Excitation of nonradiative surface plasma waves in silver by the method of frustrated total reflection, Z. fur Phys. 216 (1968) 398.
[14] B.D. Gupta, A.M. Shrivastav, S.P. Usha, Surface plasmon resonancebased fiber optic sensors utilizing molecular imprinting, Sensors 16 (2016) 1381.
[15] C. Caucheteur, T. Guo, F. Liu, B. Guan, J. Albert, Ultrasensitive plasmonic sensing in air using optical fibre spectral combs, Nat. Commun. 7 (2016) 13371.
[16] W. Liu, C.J. Hu, L. Zhou, Z. Yi, C. Liu, J.W. Lv, L. Yang, P.K. Chu. A square-lattice D-shaped photonic crystal fiber sensor based on SPR to detect analytes with large refractive indexes, Phys. E. 138 (2022), 115106.
[17] W. Liu, C. Liu, J.X. Wang, J.W. Lv, Y. Lv, L. Yang, N. An, Z. Yi, Q. Liu, C.J. Hu, P.K. Chu, Surface plasmon resonance sensor composed of microstructured optical fibers for monitoring of external and internal environments in biological and environmental sensing, Results Phys. 47 (2023), 106365.
[18] A.A. Rifat, R. Ahmed, G.A. Mahdiraji, A. Mahamd, F.R.M. Adikan, Highly sensitive D-shaped photonic crystal fiber-based plasmonic biosensor in visible to Near-IR, IEEE Sens. J. 17 (9) (2017) 2776–2783.
[19] R.A. Kadhim, L. Yuan, W. Jiang, Optical fiber refractive index sensor based on the SPR using a multiple D-shaped Ag nanowire, IEEE Sens. 25–28 (2020) 20258281.
[20] W. Liu, C.J. Hu, L. Zhou, Z. Yi, Y. Shi, C. Liu, J.W. Lv, L. Yang, A highly sensitive D-type photonic crystal fiber infrared sensor with indium tin oxide based on surface plasmon resonance, Mod. Phys. Lett. B. 36 (1) (2022) 2150499.
[21] J.W. Wang, C. Liu, F.M. Wang, W.Q. Su, L. Yang, J.W. Lv, G.L. Fu, X.L. Li, Q. Liu, T. Sun, Surface plasmon resonance sensor based on coupling effects of dual photonic crystal fibers for low refractive indexes detection, Results Phys. Volume 18 (103240) (2020) 2211–3797.
[22] Y. Zhan, Y. Li, Z. Wu, et al., Surface plasmon resonance-based microfiber sensor with enhanced sensitivity by gold nanowires, Opt. Mater. Express 8 (12) (2018) 3927–3940.
[23] L. Zhao, H. Han, N. Luan, et al., A temperature plasmonic sensor based on a side opening hollow fiber filled with high refractive index sensing medium, Sensors 19 (17) (2019) 3730.
[24] A.K. Pathak, B.M.A. Rahman, C. Viphavakit, Nanowire embedded micro-drilled dual-channel approach to develop highly sensitive biosensor, IEEE Photonics Technol. Lett. 34 (13) (2022) 707–710.
[25] C. Liu, G.L. Fu, F.M. Wang, Z. Yi, C.H. Xu, L. Yang, Q. Liu, W. Liu, X.L. Li, H.W. Mu, T. Sun, P.K. Chu, Ex-centric core photonic crystal fiber sensor with gold nanowires based on surface plasmon resonance, Opt., Vol. 196 163173 (2019) 0030–4026.
[26] C. Liu, L. Yang, Q. Liu, et al., Analysis of a surface plasmon resonance probe based on photonic crystal fibers for low refractive index detection,J, Plasmonics 13 (2018) 779–784.
[27] K. Tong, Z. Cai, J. Wang, et al., D-type photonic crystal fiber sensor based on metal nanowire array, Optik 218 (2020), 165010.
[28] R.A. Kadhim, J. Wu, Z. Wang, Sensitivity enhancement of a plasmonic sensor based on a side opening quasi-D-shaped optical fiber with Au nanowires, J. Opt.-UK (2021) 1–8.
[29] J. Banerjee, S. Mandal, M. Pradhan, Polarization-multiplexed incoherent broadband surface plasmon resonance: a new analytical strategy for plasmonic sensing, Anal. Chem. 18 (2022) 94.
[30] P. Jia, J. Yang, Integration of large-area metallic nanohole arrays with multimode optical fibers for surface plasmon resonance sensing, Appl. Phys. 102 (24) (2013) 667.

[31] G. Kumar, V.K. Tripathi, Anomalous absorption of surface plasma wave by particles adsorbed on metal surface, Appl. Phys. 91 (16) (2007), 134108.
[32] Z. Samavati, A. Samavati, A.F. Ismail, et al., Optical fiber sensor for glycoprotein detection based on localized surface plasmon resonance of discontinuous Ag-deposited nanostructure, Opt. Fiber Technol. 62 (2) (2021), 102476.
[33] C. Liu, J.W. Lv, W. Liu, F.M. Wang, P.K. Chu, Overview of refractive index sensors comprising photonic crystal fibers based on the surface plasmon resonance effect [Invited], Chin. Opt. Lett. 19 (10) (2021), 102202.
[34] W. Liu, C.J. Hu, L. Zhou, Z. Yi, C. Liu, J.W. Lv, L. Yang, P.K. Chu, Ultra-sensitive hexagonal PCF-SPR sensor with a broad detection range, J. Mod. Opt. 67 (20) (2020) 1545–1554.
[35] W. Liu, F.M. Wang, C. Liu, L. Yang, Q. Liu, W.Q. Su, J.W. Lv, S.N. An, X.L. Li, T. Sun, P.K. Chu, A hollow dual-core PCF-SPR sensor with gold layers on the inner and outer surfaces of the thin cladding, Results Opt. 1 (2020), 100004.
[36] L. Duan, X. Yang, Y. Lu, J. Yao, Hollow-fiber-based surface plasmon resonance sensor with large refractive index detection range and high linearity, Appl. Optic 56 (36) (2017) 9907–9912.
[37] A.K. Mishra, S.K. Mishra, B.D. Gupta, SPR based fiber optic sensor for refractive index sensing with enhanced detection accuracy and figure ofmerit in visible region, Opt. Commun. 344 (2015) 86–91.
[38] H.N. Rafi, M.R. Kaysir, M.J. Islam, Air-hole attributed performance ofphotoniccrystal fiber-based SPR sensors, Sens. Bio-Sens. Res 29 (2020), 100364.
[39] M.R. Momota, M.R. Hasan, Hollow-core silver coated photonic crystal fiber plasmonic sensor, Opt. Mater. 76 (2018) 287–294.
[40] E. Haque, M.A. Hossain, F. Ahmed, Y. Namihira, Surface plasmon resonance sensor based on modified D-shaped photonic crystal fiber for wider range of refractive index detection, IEEE Sens. J. (2018), 1-1.
[41] V. Kaur, S. Singh, Design of titanium nitride coated PCF-SPR sensor for liquid sensing applications, Opt. Fiber Technol. 48 (2019) 159–164.
[42] Y. Wang, J. Dai, M. Zhang, et al., Theoretical and experimental study on multimode optical fiber grating, Opt. Commun. 250 (1–3) (2005) 54–62.
[43] J. Lv, H. Fu, C. Hu, et al., Double-formant surface plasmon resonance for refractive index sensing by anti-resonance fibers with high sensitivity and wide detection range, Results Phys. 40 (2022), 105876.
[44] B.H. Almewafy, N.F.F. Areed, M.F.O. Hameed, S.S.A. Obayya, Modifed D-shaped SPR PCF polarization filter at telecommunication wavelengths, Opt. Quant. Electron. 51 (6) (2019) 1–14.
[45] G. Xiao, J. Su, H. Yang, et al., Fiber optic sensor with a gold nanowire group array for broad range and low refractive index detection, Photon. MDPI 9 (9) (2022) 661.